Macromolecules

Article

pubs.acs.org/Macromolecules

Various Digital Memory Behaviors of Functional Aromatic Polyimides Based on Electron Donor and Acceptor Substituted Triphenylamines

Yong-Gi Ko,[†,§] Wonsang Kwon,[†,§] Hung-Ju Yen,[‡,§] Cha-Wen Chang,[‡,§] Dong Min Kim,[†] Kyungtae Kim,[†] Suk Gyu Hahm,[†] Taek Joon Lee,[†] Guey-Sheng Liou,[*,‡] and Moonhor Ree[*,†]

[†]Department of Chemistry, Division of Advanced Materials Science, Pohang Accelerator Laboratory, Center for Electro-Photo Behaviors in Advanced Molecular Systems, BK School of Molecular Science, and Polymer Research Institute, Pohang University of Science & Technology (POSTECH), Pohang 790-784, Republic of Korea

[‡]Institute of Polymer Science and Engineering, National Taiwan University, Taipei 10617, Taiwan

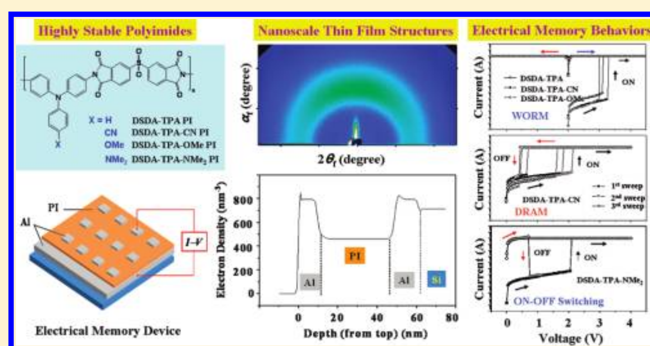

ABSTRACT: A series of aromatic polyimides (PIs) were synthesized via the polymerization of 3,3′,4,4′-diphenylsulfonyltetracarboxylic dianhydride with 4,4′-diaminotriphenylamine derivatives containing hydrogen, cyano, methoxy, or dimethylamine substituents. These PIs were thermally and dimensionally stable and produced high-quality thin films when applied in a conventional spin-coating process. Their structure and properties were characterized. Nanoscale thin films of the PIs demonstrated excellent electrical memory performance, with high stabilities and ON/OFF current ratios. The memory characteristics were found to be tunable by varying the substituents; nonvolatile write-once−read-many-times memory behavior, nonvolatile ON/OFF switching type memory behavior, and volatile dynamic random access memory behavior were observed. The memory characteristics were substantially influenced by the electron-accepting cyano- and electron-donating dimethylamine substituents but were apparently not affected by the electron-donating methoxy substituent. In addition, the film density was a significant factor influencing the observed memory behaviors, with larger film densities causing lower OFF-current levels. However, the critical switching-on voltage varied very little as the substituents were changed and was measured to be approximately ±2 V. All of the memory behaviors were found to be governed by a mechanism involving trap-limited space-charge-limited conduction and local filament formation. Overall, all of the PIs assessed in the present work were found to be suitable active materials for the low-cost mass production of high-performance, programmable unipolar memory devices that can be operated with very low power consumption, high ON/OFF current ratios, and high thermal and dimensional stability.

■ INTRODUCTION

Aromatic polyimides (PIs) are known to possess excellent thermal stability, dimensional stability, and mechanical properties.[1−5] Because of these advantageous properties, PIs have found diverse applications in the microelectronics, flat panel display, aerospace, and chemical and environmental industries as flexible circuitry carriers, stress buffers, interdielectric layers, passivation layers, liquid crystal alignment layers, varnishing resins, fibers, matrix materials, and gas and chemical separation membranes.[1−5]

Recently, PIs have been considered as candidates for active memory materials in high performance volatile and nonvolatile memory devices because of their high thermal and dimensional stability.[6−12] As a result, several new PIs have been reported for the fabrication of memory devices; these PIs contain anthracene,[6] carbazole,[7] diphenylamine,[8] and triphenylamine (TPA)[9] and its derivatives.[10−12] Interestingly, these materials displayed a variety of memory behaviors, including nonvolatile write-once−read-many-times (WORM) (i.e., fuse-type) memory, nonvolatile ON−OFF switchable memory, and volatile memory (i.e., dynamic random access memory (DRAM)) behaviors, with the behaviors displayed depending on the chemical structure as well as the film thickness.[6−12] Moreover, these memory behaviors were unipolar and/or bipolar, depending on the chemical structure.[6−12] The results showed that the electrical memory behavior of PIs is primarily dependent upon their chemical nature (including active functional groups). To facilitate the development of high-performance memory polyimides, it is therefore essential to understand the relationship between their electrical memory behavior and their chemical structure; at present, this relationship is not well understood, and the development of high-performance polyimides for memory devices remains in its early stages.

In the present study, we synthesized a series of aromatic PIs bearing TPA moieties with electron donor and acceptor groups and sought to determine the effects of the electron donor and acceptor groups on the electrical memory characteristics: poly(4,4′-aminotriphenylene 3,3′,4,4′-diphenylsulfonyltetracarboximide)

Received: February 14, 2012
Revised: April 8, 2012
Published: April 18, 2012

ACS Publications © 2012 American Chemical Society

(DSDA-TPA PI), poly(*N*-(4-cyanophenyl)-*N*,*N*-4,4′-diphenylene 3,3′,4,4′-diphenylsulfonyltetracarboximide) (DSDA-TPA-CN PI), poly(*N*-(4-methoxyphenyl)-*N*,*N*-4,4′-diphenylene 3,3′,4,4′-diphenylsulfonyltetracarboximide) (DSDA-TPA-OMe PI), and poly(*N*-(4-(dimethylamino)phenyl)diphenylene 3,3′,4,4′-diphenylsulfonyltetracarboximide) (DSDA-TPA-NMe_2 PI) (Figure 1a). Interestingly, the PIs used in our study were found to exhibit various memory behaviors (ON/OFF switching type memory, WORM memory, and DRAM) with unipolar characteristics, depending on the electron donor and acceptor substituents. The switching mechanism was also investigated. In addition, the interfaces between the PI films and the metal electrodes in the devices were examined.

■ EXPERIMENTAL SECTION

4,4′-Diaminotriphenylamine (TPA; melting point (mp): 186−187 °C), 4,4′-diamino-4″-methoxytriphenylamine (TPA-OMe; mp: 150−152 °C), 4,4′-diamino-4″-cyanotriphenylamine (TPA-CN; mp: 227−229 °C), and 4,4′-diamino-4″-*N*-(4-dimethylamino)triphenylamine (TPA-NMe_2; mp: 177−178 °C) were synthesized, according to the previously reported procedure,[13] from cesium fluoride or sodium hydride-assisted nucleophilic displacement reaction of 4-fluoronitrobezene with aniline, *p*-anisidine, 4-aminobenzonitrile, and *N*,*N*-dimethyl-*p*-phenylenediamine, respectively, followed by hydrazine Pd/C-catalyzed reduction. Elemental analysis as well as infrared and nuclear magnetic resonance spectroscopy analysis was used to determined purity and structures of the intermediate dinitro compounds and the targeted diamine monomers. DSDA-TPA PI was prepared from 3,3′,4,4′-diphenylsulfonyltetracarboxylic dianhydride (DSDA) and TPA according to the synthetic procedure reported in the literature.[13] In a similar manner, DSDA-TPA-CN PI, DSDA-TPA-OMe PI, and DSDA-TPA-NMe_2 PI were synthesized from the polymerizations of DSDA with TPA-CN, TPA-OMe, and TPA-NMe_2, respectively.

For the obtained PIs, inherent viscosities were determined with a concentration of 0.5 g/dL in *N*-methyl-2-pyrrolidinone (NMP) 30 °C using a Tamson TV-2000 viscometer. Furthermore, for some selected PIs, molecular weights were measured at 70 °C using a gel permeation chromatography (GPC) system (Lab Alliance RI2000 Instruments) connected with a refractive index detector (Schambeck SFD Gmbh). The GPC system was calibrated with polystyrene standards; *N*,*N*-dimethylformamide (DMF) was used with a flow rate of 1 mL/min as the eluent. Thermal properties were measured in a nitrogen atmosphere using a thermogravimetric analyzer (Perkin-Elmer Pyris 1 TGA), a differential scanning calorimeter (Perkin-Elmer Pyris Diamond DSC), and a thermomechanical analyzer (Perkin-Elmer TMA 7). A heating rate of 20 °C/min was employed.

Optical properties were measured using an ultraviolet−visible (UV−vis) spectrometer (Scinco model S-3100). Cyclic voltammetry (CV) was carried out in 0.1 M tetrabutylammonium tetrafluoroborate in acetronitrile (CH_3CN) by using an electrochemical workstation (IM6ex impedance analyzer) with a platinum gauze counter electrode and an Ag/AgCl (saturated KCl) reference electrode, and the polymer was coated on the gold (Au) electrode deposited on silicon substrate. A scan rate of 100 mV/s was used.

For the fabrication of memory devices, homogeneous PI solutions (1.0 wt %) were prepared in cyclopentanone and then filtered using polytetrafluoroethylene-membrane-based (PTFE) microfilters with a pore size of 0.20 μm. Single active-layer memory devices (Figure 1b) were then fabricated as follows. The polymer solutions were spin-coated onto the glasses and silicon substrates deposited with aluminum (Al) layer (with a thickness of 300 nm) by electron beam sputtering at 2500 rpm for 45 s. The PI films were then baked at 80 °C for 5 h in vacuum. The thicknesses of the PI films were determined by using a spectroscopic ellipsometer (model M2000, Woollam). The Al top electrodes with a thickness of 300 nm were deposited onto the polymer films through a shadow mask by means of thermal evaporation, with a size of 0.3 × 0.3 and 0.5 × 0.5 mm^2. All electrical

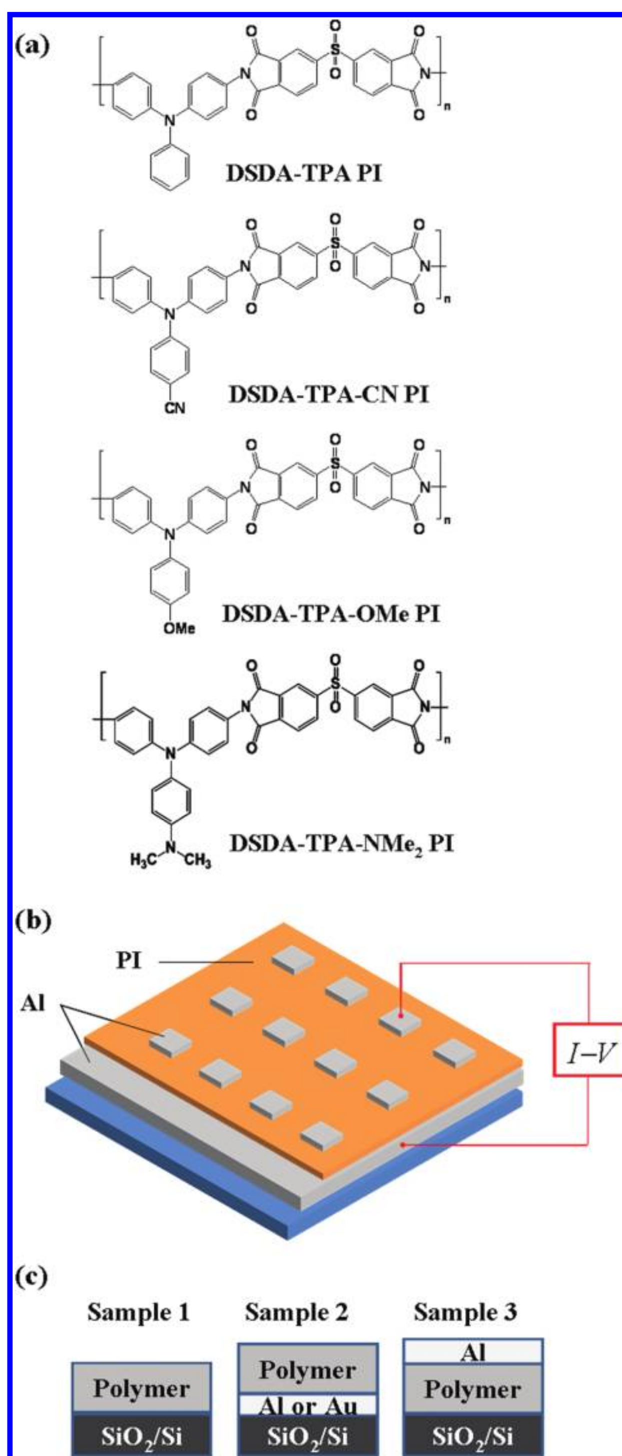

Figure 1. (a) Chemical structure of polyimides bearing four different triphenylamine derivatives: DSDA-TPA PI, DSDA-TPA-CN PI, DSDA-TPA-OMe PI, and DSDA-TPA-NMe_2 PI. (b) A schematic diagram of the memory devices fabricated with nanoscale thin films of the PIs and aluminum (Al) top and bottom electrodes. (c) Schematic diagrams of three types of samples for X-ray reflectivity measurements.

experiments were conducted without any device encapsulation either in ambient condition or in nitrogen atmosphere. Current−voltage (*I*−*V*) measurements were carried out using a Keithley 4200-SCS semiconductor analyzer and a probe station equipped with a heating stage. In all cases, bias voltage was applied with respect to the bottom electrode. Atomic force microscopy (AFM) surface images were obtained using a tapping mode atomic force microscope (Digital

Instruments, model Multimode AFM Nanoscope IIIa); a cantilever (with a 26 N/m spring constant and 268 K Hz resonance frequency) was used. X-ray reflectivity (XR) data were measured at the 3C2 beamline of the Pohang Light Source.[14] Samples were mounted on a Huber four-circle goniometer, and a scintillation counter with an enhanced dynamic range (Bede Scientific, EDR) was used as a detector. The measured reflected intensities were normalized to the intensity of the incident beam, which was monitored using an ionization chamber. For XR experiments, we prepared three kinds of samples for each polymer as shown in Figure 1c: (i) 30 nm thick PI films on silicon (Si) substrates with native oxide layer; (ii) 30 nm thick PI films on the 10 nm thick Al or Au electrodes which were deposited on Si substrates by electron-beam sputtering; (iii) thermally evaporated 10 nm thick Al electrodes on the 30 nm thick PI films coated onto Si substrates.

Grazing-incidence X-ray scattering (GIXS) measurement was performed at the 4C2 beamline of the Pohang Light Source.[15,16] Measurements were performed at a sample-to-detector distance (SDD) of 125 mm for grazing incidence wide-angle X-ray scattering (GIWAXS) and 2220 mm for grazing incidence small-angle X-ray scattering (GISAXS). Scattering data were typically collected for 30 s using X-ray radiation source of $\lambda = 0.138$ nm with a two-dimensional charge-coupled detector (Roper Scientific, Trenton, NJ). The incidence angle α_i of the X-ray beam was set at 0.147° for wide-angle scattering and 0.159° for small-angle scattering, respectively, which are between the critical angle of the PI film and the silicon substrate ($\alpha_{c,f}$ and $\alpha_{c,s}$). With these incidence angles, the X-ray beam can penetrate into the whole PI film layers. Scattering angles were corrected according to the positions of the X-ray beams reflected from the silicon substrate with respect to a precalibrated silver behenate (TCI, Japan) powder. Aluminum foil pieces were applied as a semitransparent beam stop because the intensity of the specular reflection from the substrate was much stronger than the scattering intensity of the polymer films near the critical angle.

■ RESULTS AND DISCUSSION

For the synthesized PIs, we measured inherent viscosity (η_{inh}), weight-average molecular weight ($\bar{M}_w$), polydispersity index (PDI), and thermal properties. The results are listed in Table 1.

Table 1. Inherent Viscosities, Molecular Weights, and Thermal Properties of the Synthesized Polyimides

polyimide	η_{inh}[a] (dL/g)	$\bar{M}_w$[b]	PDI[c]	T_g[d] (°C)	T_d^{10}[e] (°C)
DSDA-TPA PI	0.50	58 000	1.39	306	540
DSDA-TPA-CN PI	0.42			325	575
DSDA-TPA-OMe PI	0.44	58 000	1.34	304	515
DSDA-TPA-NMe_2 PI	0.43			331	520

[a]Inherent viscosity measured at a polymer concentration of 0.5 g/dL in NMP at 30 °C. [b]Weight-average molecular weight measured at 70 °C using a GPC system calibrated with polystyrene standards; DMF was used as the eluent. [c]Polydispersity index (= $\bar{M}_w/\bar{M}_n$) measured by GPC analysis. [d]Glass transition temperature measured with a heating rate of 10 °C/min in nitrogen atmosphere by thermomechanical analysis. [e]Temperature at which 10 wt % weight loss occurred in nitrogen atmosphere. A heating rate of 20 °C/min was employed.

The measured η_{inh} values ranged in 0.42–0.50. The DSDA-TPA and DSDA-TPA-OMe PIs as the representative PIs were further considered for GPC analysis in order to get information about the relationship between the inherent viscosities and molecular weights of the polymers. The measured $\bar{M}_w$ and PDI were 58 000 and 1.39 for DSDA-TPA PI and 58 000 and 1.34 for DSDA-TPA-OMe PI, respectively. These results collectively indicate that all the PIs were synthesized with reasonably high molecular weights.

The thermal degradation temperature T_d^{10} (which caused 10 wt % weight loss) in a nitrogen atmosphere was found to be 540 °C for DSDA-TPA PI, 575 °C for DSDA-TPA-CN PI, 515 °C for DSDA-TPA-OMe PI, and 520 °C for DSDA-TPA-NMe_2 PI. The glass transition temperature T_g was measured to be 306 °C for DSDA-TPA PI, 325 °C for DSDA-TPA-CN PI, 304 °C for DSDA-TPA-OMe PI, and 331 °C for DSDA-TPA-NMe_2 PI. DSDA-TPA PI has no substituent and, thus, shows relatively higher degradation temperature than those of DSDA-TPA-OMe and DSDA-TPA-NMe_2 PIs. Interestingly DSDA-TPA-CN PI exhibits the highest degradation temperature although it contains one cyano substituent per repeat unit. In contrast, DSDA-TPA-NMe_2 PI, which contains one dimethylaminine substituent per repeat unit, reveals relatively higher T_g than those of DSDA-TPA PI and the other PIs. In comparison, the T_g of DSDA-TPA PI was increased by the dimethylamine and cyano substituents but reduced by the methoxy substituent. Overall, the thermal and dimensional stabilities are comparable to those of conventional aromatic PIs.

The PI films were investigated by UV–vis spectroscopy and CV analysis. The PIs in thin films showed the longest absorption maximum λ_{max} in the range of 325–360 nm (Figure 2a–d). The λ_{max} value is in the increasing order DSDA-TPA-CN PI < DSDA-TPA PI < DSDA-TPA-OMe PI < DSDA-TPA-NMe_2 PI, indicating that for the UV–vis absorption of DSDA-TPA PI, the methoxy and dimethylamino substituents (electron donor groups) cause red shifts while the cyano substituent (an electron acceptor group) induces a blue shift. From the UV–vis spectra, the band gap (i.e., the difference between the highest occupied molecular orbital (HOMO) level and the lowest unoccupied molecular orbital (LUMO) level for the polymer) was estimated to be 3.04 eV for DSDA-TPA PI, 3.17 eV for DSDA-TPA-CN PI, 2.99 eV for DSDA-TPA-OME PI, and 2.91 eV for DSDA-TPA-NMe_2 PI. The oxidation half-wave potentials ($E_{1/2}$) vs Ag/AgCl was determined to be 1.11 V for DSDA-TPA PI, 0.87 V for DSDA-TPA-CN PI, 0.95 V for DSDA-TPA-OME PI, and 0.54 eV for DSDA-TPA-NMe_2 PI (Figure 2A–C). The external ferrocene/ferrocenium (F_c/F_{c+}) redox standard potential, $E_{1/2}(F_c/F_{c+})$, was measured to be 0.59 V vs Ag/AgCl in acetonitrile. Assuming that the HOMO level for the F_c/F_{c+} standard is −4.80 eV with respect to the zero vacuum level, the HOMO level of each PI was estimated from the measured $E_{1/2}$ data. The LUMO level of each PI was calculated from the obtained optical band gap and HOMO level. The determined HOMO and LUMO levels were −5.32 and −2.28 eV for DSDA-TPA PI, −5.08 and −1.94 eV for DSDA-TPA-CN PI, −5.16 and −2.17 eV for DSDA-TPA-OMe PI, and −4.75 and −1.84 eV for DSDA-TPA-NMe_2 PI, respectively. These results indicate that the substituent of the TPA unit influences the HOMO and LUMO levels of DSDA-TPA PI. Overall, all the substituents caused to increase both the HOMO level and the LUMO level. It turns out that the electron-donating methoxy and dimethylamine substituents slightly reduced the band gap and, however, the electron-withdrawing cyano substituent increased the band gap.

The PI films deposited on silicon substrates and metal electrodes were examined by AFM analysis. Representative AFM images are shown in Figure 3, which were measured for the DSDA-TPA PI films. The DSDA-TPA PI polymer films coated on silicon substrates were determined to have a root-mean-square (rms) roughness of 0.26 nm over an area of 1.0 × 1.0 μm^2

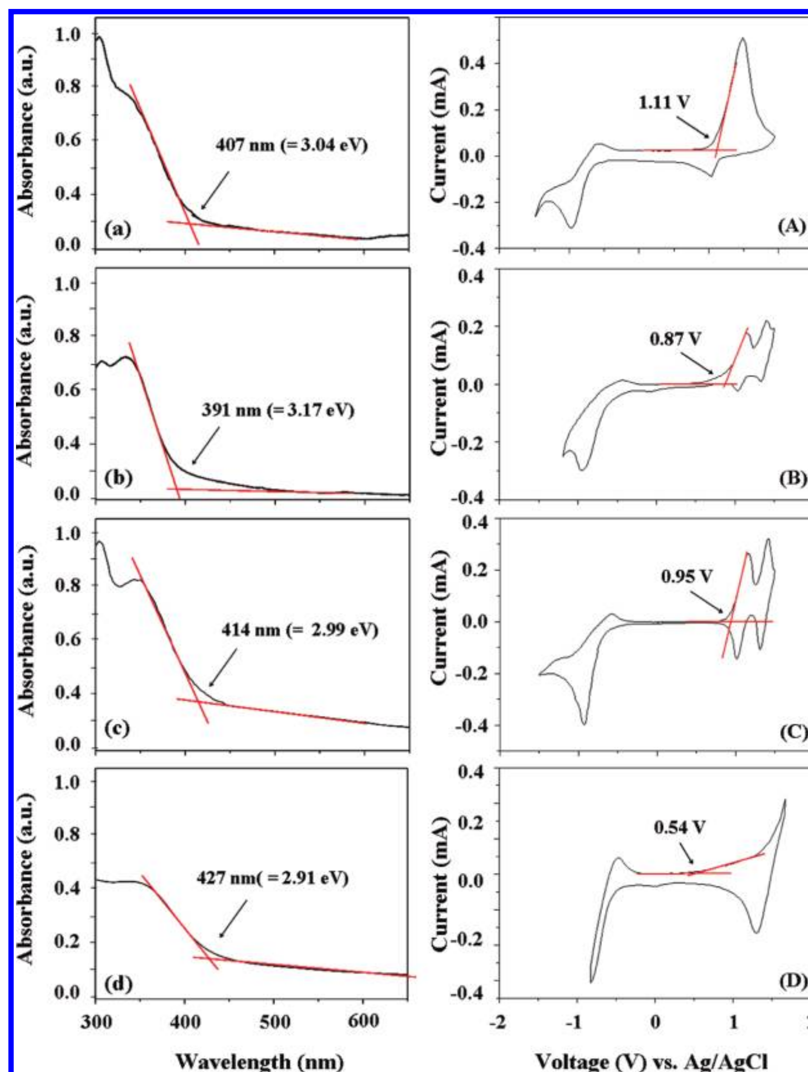

Figure 2. UV−vis spectra and CV responses of the PIs films which were coated on quartz substrates and fabricated with Au electrodes supported by silicon substrates respectively: (a, A) DSDA-TPA PI; (b, B) DSDA-TPA-CN PI; (c, C) DSDA-TPA-OMe PI; (d, D) DSDA-TPA-NMe_2 PI. The CV measurements were carried out in aqueous 0.1 M tetrabutylammonium tetrafluoroborate in acetonitrile using an electrochemical workstation with a platinum gauze counter electrode and an Ag/AgCl (3.8 M KCl) reference electrode. A scan rate of 100 mV/s was used.

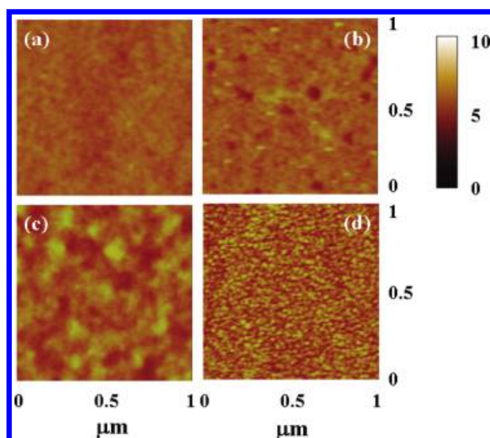

Figure 3. Representative AFM surface images: (a) DSDA-TPA PI film coated on Si substrate; (b) Al bottom electrode deposited on Si substrate; (c) DSDA-TPA PI film coated on Au bottom electrode; (d) Al electrode (10 nm thick) deposited on the DSDA-TPA PI film supported with Si substrate.

(Figure 3a). In comparison, an rms roughness was measured to be 0.45 nm for the DSDA-TPA-CN PI films and 0.24 nm for the DSDA-TPA-OMe and DSDA-TPA-NMe_2 PI films. For the films coated on the Al bottom electrodes, the rms surface roughness was 0.75 nm for DSDA-TPA PI (Figure 3b), 0.69 nm for DSDA-TPA-CN PI, 0.41 nm for DSDA-TPA-OMe PI, and 0.45 nm for the DSDA-TPA-NMe_2 PI films. For the films coated on the Au bottom electrodes, the rms surface roughness was 0.63 nm for DSDA-TPA PI (Figure 3c), 0.60 nm for DSDA-TPA-CN PI, and 0.60 nm for DSDA-TPA-OMe PI. Here, the Al and Au electrodes were measured to have rms surface roughnesses of 0.1−1.3 nm before the PI depositions. The Al top electrodes deposited on the DSDA-TPA PI films were determined to have an rms surface roughness of 0.70−0.73 nm (Figure 3d). Similar surface roughnesses were measured for the Al top electrodes deposited on films of the other three PIs. Collectively these results confirm that the PI polymers dissolved in cyclopentanone produce high quality nanoscale thin films with smooth surface via solution coating on silicon substrates and metal electrodes and subsequent drying process.

Morphological structures of the thin PI films (ca. 30 nm thick) deposited on silicon substrates were investigated by synchrotron GISAXS and GIWAXS analysis. The DSDA-TPA PI films showed featureless GISAXS pattern (Figure 4a).

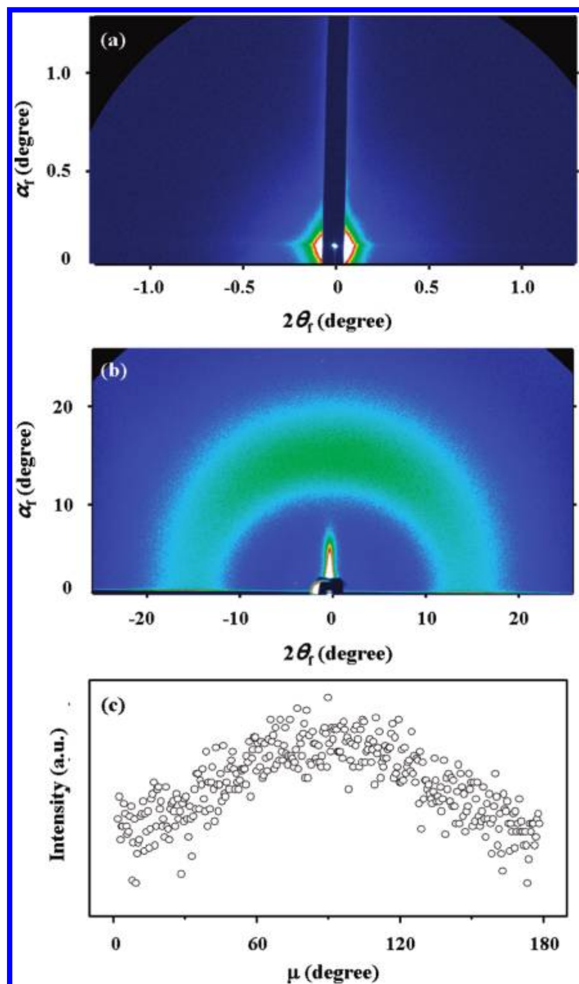

Figure 4. (a) Synchrotron 2D GISAXS pattern measured at 25 °C with α_i = 0.159° for a 30 nm thick 6F-HAB-AM PI film deposited on a silicon substrate. (b) 2D GIWAXS pattern measured with α_i = 0.147°. (c) Azimuthal scattering profile extracted from the 2D GIWAXS pattern in (b) along the amorphous halo ring.

However, the films revealed only one weak, broad ring scattering in the GIWAXS pattern (Figure 4b). This ring was determined to have a *d*-spacing of 0.490 nm, which corresponds to the mean interdistance of the polymer chains. The scattering ring was slightly anisotropic in intensity toward the meridian line (Figure 4b,c). This scattering result indicates that in the thin film the polymer chains orient somewhat preferentially in the film plane rather than randomly. Similar GISAXS and GIWAXS patterns were observed for the other three PIs (data not shown). From the anisotropic ring scattering, the *d*-spacing was determined to be 0.512 nm for the DSDA-TPA-CN PI films, 0.506 nm for the DSDA-TPA-OMe PI films, and 0.491 nm for the DSDA-TPA-NMe$_2$ PI films.

In the memory devices, the PIs were in physical contact with the metal electrodes. The PI films in contact with the metal electrodes and the silicon substrates were further studied using synchrotron XR analysis. Representative XR profiles of the DSDA-TPA PI films are shown in Figure 5. Similar XR data

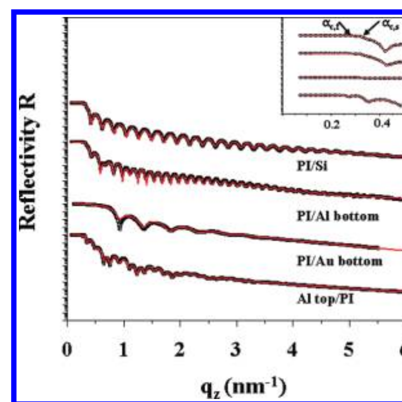

Figure 5. Representative XR profiles of DSDA-TPA PI films (ca. 30 nm thick) in contact with silicon substrate, Al bottom electrode, Au bottom electrode (ca. 10 nm thick), and Al top electrode (ca. 10 nm thick). The symbols are the measured data, and the solid line represents the fit curve assuming a homogeneous electron density distribution within the film. The inset shows a magnification of the region around the two critical angles: $\alpha_{c,f}$ and $\alpha_{c,s}$ are the critical angles of the film and the substrate (silicon substrate or Al electrode), respectively.

were obtained for the films of the other three PIs (data not shown). All of the XR data were satisfactorily fitted using the Parratt algorithm.[17] The analysis results are summarized in Table 2. For the PI films deposited on the silicon substrates, the electron density ρ_e was 460.9 nm^{-3} for the DSDA-TPA PI, 425.8 nm^{-3} for the DSDA-TPA-CN PI, 426.9 nm^{-3} for the DSDA-TPA-OMe PI, and 462.7 nm^{-3} for the DSDA-TPA-NMe$_2$ PI. These results indicated that the electron density of the DSDA-TPA PI film was slightly reduced by the incorporation of methoxy or cyano substituents but was apparently not influenced by the incorporation of dimethylamine substituents. These ρ_e values were correlated with the *d*-spacing values (i.e., the interdistances of the PI polymer chains) determined in the aforementioned GIWAXS analysis. The determined ρ_e values were reasonably consistent with values measured for PI films deposited on Al and Au bottom electrodes and Al top electrodes. These results indicated that no aluminum atoms or ions diffused into the PI film layers during the deposition of the PI films on the Al bottom electrode. However, an interlayer with a thickness of 0.3−1.2 nm was detected for the PI films deposited on Al bottom electrodes. The thin interlayer was determined to have a root-mean-square (rms) roughness of 0.3−1.1 nm. The ρ_e values were determined to be in the range of 886.8−1229.8 nm^{-3}; these ρ_e values are larger than that of aluminum. These results suggest that a thin aluminum oxide layer was formed on the Al bottom electrodes during the deposition of the PI films on the bottom electrodes.

An interlayer was also determined to be present for the Al top electrodes deposited on the PI films. Its thickness ranged from 0.9 to 1.2 nm, values comparable to the surface roughnesses of the PI films. The presence of the thin interfacial layer was therefore attributed to the mechanical mixing of the two layers that occurred in the rough surface of the PI film. The roughness of the PI films might have originated from the bombardment of the surface of the polymer film with high thermal energy Al atoms and their aggregates during the thermal evaporation process. The ρ_e values were determined to be 440.8−528.7 nm^{-3}; these values are closer to those of the PI films than that of aluminum or aluminum oxide. These results

dx.doi.org/10.1021/ma300311d | *Macromolecules* 2012, 45, 3749−3758

Table 2. Structural Parameters and Electron Density Profiles of Various Bilayer Samples Prepared from the PI Films, Silicon Substrates, Al Electrodes, and Au Electrodes

sample (top/bottom)	bottom layer			PI layer			top layer			interlayer[d]		
	d^a (nm)	$\rho_e{}^b$ (nm^{-3})	σ^c (nm)	d^a (nm)	$\rho_e{}^b$ (nm^{-3})	σ^c (nm)	d^a (nm)	$\rho_e{}^b$ (nm^{-3})	σ^c (nm)	d^a (nm)	$\rho_e{}^b$ (nm^{-3})	σ^c (nm)
DSDA-TPA PI												
PI/Si		714.5	0.1	27.0	460.9	0.3				0.5	660.0	0.5
PI/Al	11.6	798.3	0.9	27.9	460.9	0.3				0.7	1155.6	0.9
PI/Au	11.2	3769.5	0.9	25.0	458.9	1.1						
Al/PI				26.7	463.6	1.5	8.7	796.7	0.3	1.2	549.8	0.6
DSDA-TPA-CN												
PI/Si		702.1	0.3	46.0	425.8	0.2				1.3	684.4	0.4
PI/Al	9.92	795.0	0.9	45.6	418.1	0.4				0.3	1127.5	1.0
PI/Au	11.0	3815.6	1.3	24.5	418.4	0.5						
Al/PI				46.01	414.9	0.1	9.3	794.2	1.2	0.9	440.8	0.3
DSDA-TPA-OMe												
PI/Si		707.4	0.8	29.6	426.9	0.7				1.8	652.1	0.4
PI/Al	12.1	767.3	1.2	29.9	426.6	0.0				1.2	1229.8	1.1
PI/Au	10.9	3741.1	1.0	24.5	432.6	1.2						
Al/PI				29.7	426.9	0.5	8.7	804.9	0.2	0.9	502.1	1.0
DSDA-TPA-NMe$_2$												
PI/Si		751.6	0.1	18.6	462.7	0.2				1.2	682.8	0.2
PI/Al	10.7	761.2	0.9	19.4	494.3	0.7				0.7	886.8	0.3
PI/Au												
Al/PI				19.2	448.5	0.8	6.1	857.3	0.8	1.0	528.7	0.5

[a]Layer thickness. [b]Electron density of layer. [c]Roughness of layer in contact with air, lower or upper layer. [d]Silicon oxide layer for Si (bottom)/PI (top), aluminum oxide layer for Al/PI, and PI−Al mixed layer (which is due to the roughness of interface) for PI/Al systems.

indicated that no aluminum oxide was formed at the interface between the PI films and the Al top electrodes during the thermal deposition of the Al top electrodes in vacuum; if aluminum oxide was formed at this interface, it is likely that the amounts were low.

To exploit these structures, properties, and film qualities, we fabricated devices with a simple Al/PI/Al structure. Figure 6 shows typical $I-V$ characteristic curves for the 30 nm thick PI films in the devices; these curves were measured using a semiconductor parameter analyzer with a compliance current of 0.01 A. All of the PI films initially exhibited a high resistance (OFF state). However, when a positive or negative voltage was applied to the PI films, they exhibited an abrupt increase in the current over the range +1.5 to +3.0 V or −1.5 to −3.0 V (which corresponds to the critical voltage $V_{c,ON}$ to switch on the device). In devices, these OFF-to-ON transitions can function as a "writing" process. After the devices reached their ON state they showed various $I-V$ characteristics, depending on both the type of PI film and the voltage sweep direction. The DSDA-TPA and DSDA-TPA-OMe PIs retained the ON state with a current compliance of 0.01 A (Figure 6a), even after the power was turned off and even during reverse and forward voltage sweeps. Specifically, these PIs displayed unipolar WORM memory behavior. Similar behavior was observed for the DSDA-TPA-CN PI films. However, for this polymer, only ~80% of the device cells showed such unipolar WORM memory behavior (Figure 6a). Interestingly, the other device cells exhibited unipolar DRAM behavior (Figure 6b). Such DRAM behavior was observed under reverse voltage sweeping or when the power was turned off. In contrast, the DSDA-TPA-NMe$_2$ PI was found to reveal quite different memory behavior. As shown in Figure 6c, the ON state remained, even after the power was turned off, or during reverse and forward voltage sweeping (with a current compliance of 0.01 A or lower). However, in the ON state, the device was switched off by applying a voltage with a current compliance of 0.1 A, which was higher than that (0.01 A) chosen in the switching-ON process. When a voltage was again applied with a current compliance of 0.1 A, there was an abrupt decrease in the current in the device near ±0.7 V, indicating that the device underwent a sharp electrical transition from the high (ON) conductivity state to the low (OFF) conductivity state.

All of the PI films revealed excellent retention abilities in both the OFF and ON state, even under ambient air conditions (Figure 7). They also exhibited high ON/OFF current ratios; the values determined were 10^7 for the DSDA-TPA PI, 10^8 for the DSDA-TPA-CN PI, 10^8 for the DSDA-TPA-OMe PI, and 10^6 for the DSDA-TPA-NMe$_2$ PI (these were measured with a reading voltage of +1.0 V).

Regarding the fabrication of the device, it was confirmed that a very thin aluminum oxide layer (with a thickness of 0.3−1.2 nm) formed on top of the Al bottom electrode during the PI film formation process. It is reasonable to postulate that the observed memory behaviors of the devices might be attributed to this thin aluminum oxide layer (in part or completely). To check this possibility, devices were fabricated and tested using Au bottom electrodes instead of Al bottom electrodes. Representative $I-V$ data from the devices with Au bottom electrodes are shown in Figure 8. They are similar to those observed for the devices with Al bottom electrodes. These results confirmed that the memory behaviors observed in the devices with Al bottom and top electrodes were not attributable to the thin aluminum oxide layer formed on the Al bottom electrodes; rather, the observed memory behaviors originated in the active PI layers in the devices.

To investigate the electrical switching characteristics of the PI films in the devices, the measured $I-V$ data were further analyzed in detail, using various conduction models; these models included Ohmic contact,[18] Schottky emission,[19]

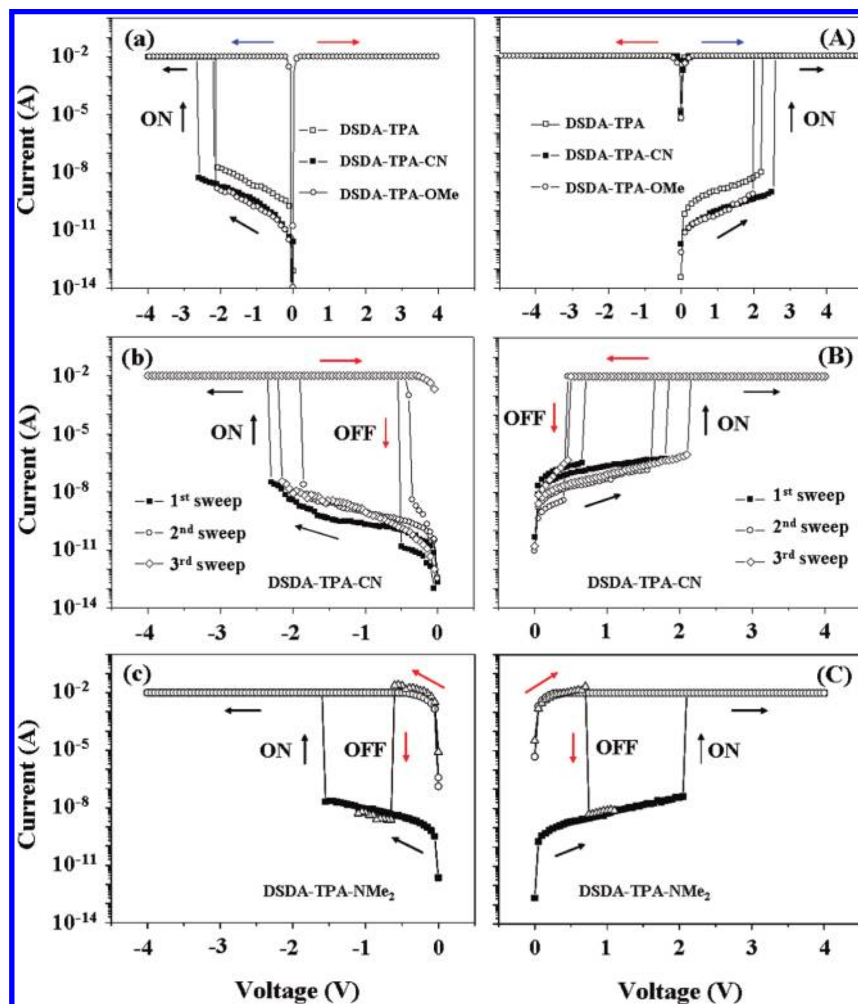

Figure 6. Typical *I*−*V* curves of the Al/PI(30 nm thick)/Al devices, which were measured with a compliance current set of 0.01 A. The applied voltage was swept from 0 to ±4.0 V. The electrode contact area was 0.5 × 0.5 mm^2. The switching-OFF runs in (c) and (C) were carried out with a compliance current set of 0.1 A.

tunneling currents,[20] space-charge limited currents,[20] and Frenkel−Poole emission.[21] The trap-limited space-charge limited conduction (SCLC) model was found to fit the *I*−*V* data for the OFF state the best (Figure 9a), while the Ohmic contact model was found to satisfactorily fit the *I*−*V* data for the ON state (Figure 9b). This showed that when the devices were in the OFF state, a trap-limited SCLC mechanism was dominant, but when the devices were in the ON state, Ohmic conduction was dominant. Moreover, the current levels in the devices in the ON state were found to be independent of the device cell size, which is indicative of heterogeneous localized filament formation. For the active PI film layers, the charge trapping sites might have arisen because of the chemical composition of the PIs. For all of the PIs, the TPA units, imide carbonyl oxygens, and sulfonyl oxygens acted as electron donors and thus as nucleophilic sites, whereas the imide carbonyl carbons and sulfonyl sulfurs acted as electron acceptors and thus as electrophilic sites. The DSDA-TPA-CN PI had one additional cyano substituent per TPA unit, which could act as an electrophilic site. The DSDA-TPA-OMe and DSDA-TPA-NMe_2 PIs had one additional methoxy substituent and one additional dimethylamine substituent per TPA unit, respectively, which were able to act as nucleophilic sites. All of these groups are likely to have acted as charge-trapping sites. Under an electrical field (i.e., when a voltage is applied), filaments are formed in polymer films by such trap sites; their response to the current flow results mainly from the hopping of charges between the traps localized in the intra- and intermolecular PI chains in the conduction paths (i.e., in the filaments).

For the devices with Al electrodes (with a work function of Φ = −4.28 eV) used in our study, the energy barrier for hole injection from the electrode to the active PI film layer (HOMO level) was estimated to be 1.04 eV for the DSDA-TPA PI, 0.80 eV for the DSDA-TPA-CN PI, 0.88 eV for the DSDA-TPA-OMe PI, and 0.47 eV for the DSDA-TPA-NMe_2 PI. The energy barrier for electron injection from the electrode to the active PI film layer (LUMO level) was estimated to be 2.00 eV for the DSDA-TPA PI, 1.34 eV for the DSDA-TPA-CN PI, 2.11 eV for the DSDA-TPA-OMe PI, and 1.64 eV for the DSDA-TPA-NMe_2 PI. All of the PI films showed a lower energy barrier for hole injection than for electron injection. These results therefore suggest that the conduction processes in the PI-based devices were dominated by hole injection. In increasing order, the energy barriers for hole injection in the films were DSDA-TPA-NMe_2 PI < DSDA-TPA-CN PI < DSDA-TPA-OMe PI < DSDA-TPA PI, as discussed above. One might therefore expect that the critical switching-ON voltage $V_{c,ON}$

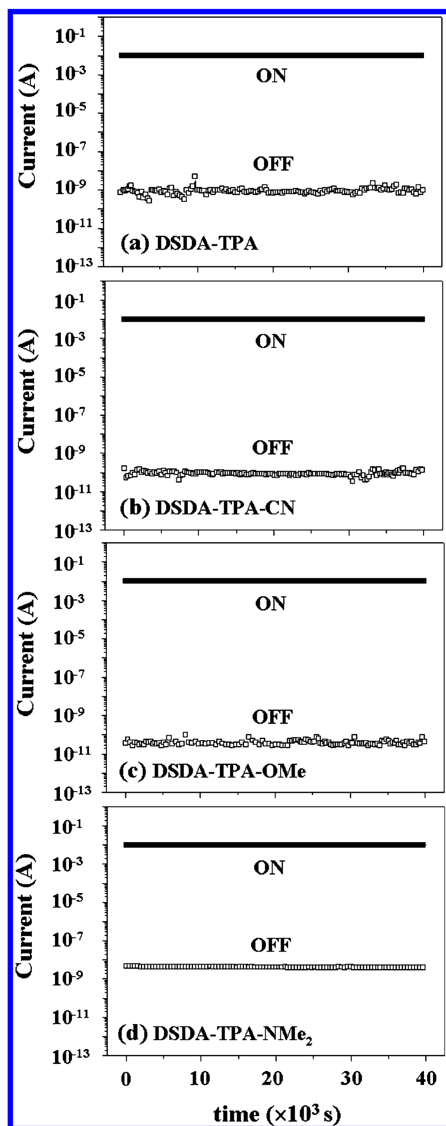

Figure 7. Retention times of the ON and OFF state of the Al/PI/Al devices, as probed with a reading voltage of +1.0 V.

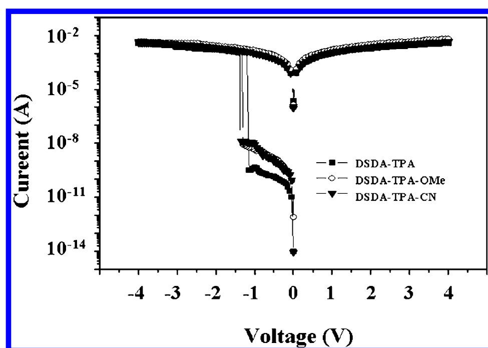

Figure 8. Typical $I-V$ curves of the Au/PI(30 nm thick)/Al devices, which were measured with a compliance current set of 0.01 A. The applied voltage was swept from 0 to ±4.0 V. The electrode contact area was 0.5 × 0.5 mm^2.

values would be in the increasing order DSDA-TPA-NMe_2 PI < DSDA-TPA-CN PI < DSDA-TPA-OMe PI < DSDA-TPA PI. However, the $V_{c,ON}$ values varied slightly around ±2 V (Figure 6). Specifically, the observed $V_{c,ON}$ values appeared to show no dependency on the electron-donating and electron-accepting substituents of the TPA units in the PIs. These results collectively suggest that the differences in the energy barriers for hole injection in the PIs could not cause discernible differences in the $V_{c,ON}$ values.

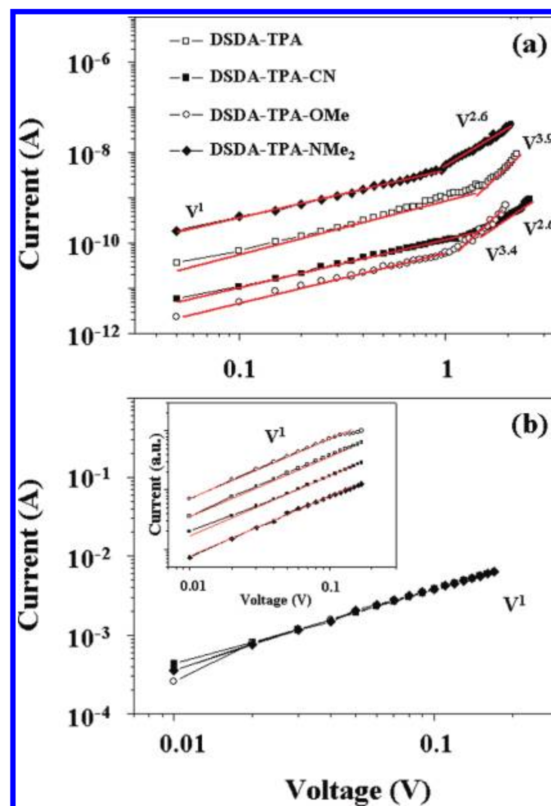

Figure 9. Experimental (symbols) and fitted (solid lines) $I-V$ curves for the Al/PI/Al devices: (a) OFF state with the Ohmic (below 1.0 V) and the trap-limited SCLC (above 1.0 V) conduction model and (b) ON state with the Ohmic current model.

In comparison, the DSDA-TPA and DSDA-TPA-NMe_2 PIs exhibited slightly higher OFF-current levels than the other two PIs (Figure 6). These PIs had higher electron densities and shorter interchain distances than the other two PIs, as discussed above. Taking these factors into account, the higher OFF-current levels of the DSDA-TPA and DSDA-TPA-NMe_2 PIs might be attributed to the higher populations of charging sites per unit volume.

Interestingly, the PIs in the devices demonstrated various memory behaviors, depending on the electron-donating and electron-accepting substituents of the TPA units (although they had the same polymer backbone). The DSDA-TPA PI exhibited unipolar WORM memory behavior. This unipolar WORM memory behavior is quite different from the bipolar DRAM characteristics reported for the devices based on poly(4,4′-aminotriphenylene hexafluoroisopropylidenediphthalimide) (6F-TPA PI).[9] The difference in the memory behaviors might be attributed to the different dianhydride units in the polymer backbones and their roles. 6F-TPA PI has two trifluormethyl groups per dianhydride unit. These have a very strong electron-accepting power because of the highly electronegative fluoro components and may thus reduce significantly the electron density at the amino group of the TPA unit, causing instability in the electrical charging and discharging behaviors and consequently leading to volatile DRAM behavior rather than nonvolatile memory behaviors. In contrast, the

dx.doi.org/10.1021/ma300311d | Macromolecules 2012, 45, 3749−3758

sulfonyl group per dianhydride unit in DSDA-TPA PI has relatively much less electron-accepting power, compared to the two trifluoromethyl groups in 6F-TPA PI, and might thus makes no significant reduction in the electron density at the TPA unit, exhibiting highly stable nonvolatile WORM memory behavior rather volatile DRAM behavior.

Surprisingly, the DSDA-TPA-CN PI showed either unipolar WORM memory behavior or unipolar DRAM behavior, depending on the device cell used (Figure 6a,b). This can be attributed to several factors arising from the incorporation of the cyano substituents. First, the incorporated cyano substituents played a role as charging sites, in addition to the TPA, imide carbonyl, and sulfonyl units discussed above. However, the cyano substituent was an electron-accepting group and thus reduced the nucleophilic power of the TPA units. Moreover, the incorporation of the cyano substituents caused a reduction in the film density, as discussed above. Because of this density reduction, the incorporation of cyano substituents led to only small increases in the number of charging sites per unit volume in the active PI film layer. Overall, these factors acted cooperatively to alter the nonvolatile memory behavior, in a negative manner.

The DSDA-TPA-OMe PI had an additional electron-donating methoxy substituent per repeat unit, and a relatively low electron density, but it revealed unipolar WORM memory behavior similar to that observed for the DSDA-TPA PI (Figure 6a). These results suggest that the methoxy substituents did not significantly influence the memory behavior. Specifically, the incorporated methoxy substituents did not perform well as charge-trapping sites. Moreover, the slight density reduction produced by the incorporated methoxy substituents did not have any significant influence on the memory behavior.

In contrast to the other PIs, the DSDA-TPA-NMe_2 PI exhibited unipolar switching memory behavior, rather than WORM memory and DRAM behaviors (Figure 6c). This result indicates that the incorporated dimethylamine substituents significantly influenced the memory behavior. The dimethylamine substituents also played a role as charge-trapping sites, in addition to the TPA, imide carbonyl, and sulfonyl units discussed above. The dimethylamine substituent was an electron-donating group and could thus strengthen the nucleophilic power of the TPA units. The film density was comparable or slightly increased compared with that of the DSDA-TPA PI, despite the fact that the dimethyl substituents were incorporated into the polymer. As a result, the incorporation of the dimethylamine substituents led to an increase in the number of charging sites per unit volume in the active PI film layer. These factors collectively influenced the memory behavior, leading to switching-type memory characteristics.

■ CONCLUSIONS

A series of DSDA-based PIs bearing four different TPA derivatives were synthesized with reasonably high molecular weights. These polymers showed high thermal and dimensional stabilities compared with conventional aromatic PIs. The polymers produced high-quality nanoscale thin films with a smooth surface when they were applied in a conventional solution coating process. All of the PIs in the films were found to be amorphous, but they were oriented somewhat preferentially in the film plane, rather than randomly. Their film densities (i.e., electron density) and interchain distances were determined, and the HOMO and LUMO levels were determined.

In the Al/PI/Al devices, all of the PIs initially exhibited a high resistance. Under positive and negative voltage sweeps, the PIs demonstrated various memory behaviors (nonvolatile WORM and switching memories and volatile DRAM), depending on the substituents of the TPA units. In addition to these substituent effects, this study showed that the film density was a significant factor in producing the observed memory behaviors. It was further found that higher film densities caused lower OFF-current levels. However, all of the PIs switched on at approximately ±2 V. They all revealed excellent retention abilities in both the OFF and ON state, even under ambient air conditions. They also exhibited high ON/OFF current ratios (10^6–10^8). All of the memory behaviors were found to be governed by a mechanism involving trap-limited SCLC conduction and local filament formation.

Overall, this study has demonstrated that thermally, dimensionally stable DSDA-TPA PI derivatives are highly suitable active materials for the low-cost mass production of high performance, polarity-free programmable memory devices that can be operated with very low power consumption, high ON/OFF current ratios, and high thermal and dimensional stability. Moreover, the memory mode can be tuned by changing the substituent in the TPA units.

■ AUTHOR INFORMATION

Corresponding Author

*E-mail ree@postech.edu, Tel +82-54-279-2120, Fax +82-54-279-3399 (M.R.); e-mail gsliou@ntu.edu.tw, Tel +886-2-3336-5315, Fax +886-2-3336-5237 (G.S.L.).

Author Contributions

[§]These authors equally contributed to this work.

Notes

The authors declare no competing financial interest.

■ ACKNOWLEDGMENTS

This study was supported by the National Research Foundation (NRF) of Korea (Doyak Program 2011-0028678 and Center for Electro-Photo Behaviors in Advanced Molecular Systems (2010-0001784)) and by the Ministry of Education, Science & Technology (MEST), Korea (BK21 Program and World Class University Program (R31-2008-000-10059-0)). This work was also supported by the National Science Council of the Republic of China (NSC 98-2113-M-002-005-MY3). Synchrotron GIXS and XR measurements were supported by MEST, POSCO, and POSTECH Foundation.

■ REFERENCES

(1) (a) Tummala, R. R., Rymaszewski, E. J., Eds.; *Microelectronics Packaging Handbook*; van Nostrand Reinhold: New York, 1989. (b) Thompson, L. F.; Willson, C. G.; Tagawa, S. *Polymers for Microelectronics: Resists and Dielectrics*; ACS. Symp. Ser. Vol. 537; American Chemical Society: Washington, DC, 1994.

(2) (a) Shin, T. J.; Ree, M. *J. Phys. Chem. B* **2007**, *111*, 13894–13900. (b) Hahm, S. G.; Lee, S. W.; Suh, J.; Chae, B.; Kim, S. B.; Lee, S. J.; Lee, K. H.; Jung, J. C.; Ree, M. *High Perform. Polym.* **2006**, *18*, 549–577. (c) Ree, M. *Macromol. Res.* **2006**, *14*, 1–33. (d) Ree, M.; Shin, T. J.; Lee, S. W. *Korea Polym. J.* **2001**, *9*, 1–19. (e) Wakita, J.; Jin, S.; Shin, T. J.; Ree, M.; Ando, S. *Macromolecules* **2010**, *43*, 1930–1941.

(3) (a) Hahm, S. G.; Lee, T. J.; Ree, M. *Adv. Funct. Mater.* **2007**, *17*, 1359–1370. (b) Hahm, S. G.; Lee, T. J.; Chang, T.; Jung, J. C.; Zin, W. C.; Ree, M. *Macromolecules* **2006**, *39*, 5385–5392. (c) Hahm, S. G.; Lee, S. W.; Lee, T. J.; Cho, S. A.; Chae, B.; Jung, Y. M.; Kim, S. B.; Ree, M. *J. Phys. Chem. B* **2008**, *112*, 4900–4912. (d) Shin, T. J.; Ree, M. *Langmuir* **2005**, *21*, 6081–6085. (e) Lee, S. W.; Lee, S. J.; Hahm, S. G.; Lee, T. J.; Lee, B.; Chae, B.; Kim, S. B.; Jung, J. C.; Zin, W. C.;

Sohn, B. H. *Macromolecules* **2005**, *38*, 4331−4338. (f) Kim, Y.; Goh, W. H.; Chang, T.; Ha, C. S.; Ree, M. *Adv. Eng. Mater.* **2004**, *6*, 39−43.

(4) (a) Lee, S. W.; Kim, S. I.; Lee, B.; Kim, H. C.; Chang, T.; Ree, M. *Langmuir* **2003**, *19*, 10381−10389. (b) Chae, B.; Lee, S. W.; Lee, B.; Choi, W.; Kim, S. B.; Jung, Y. M.; Jung, J. C.; Lee, K. H.; Ree, M. *J. Phys. Chem. B* **2003**, *107*, 11911−11916. (c) Chae, B.; Lee, S. W.; Lee, B.; Choi, W.; Kim, S. B.; Jung, Y. M.; Jung, J. C.; Lee, K. H.; Ree, M. *Langmuir* **2003**, *19*, 9459−9465. (d) Lee, S. W.; Kim, S. I.; Lee, B.; Choi, W.; Chae, B.; Kim, S. B.; Ree, M. *Macromolecules* **2003**, *36*, 6527−6536. (e) Lee, S. W.; Chae, B.; Lee, B.; Choi, W.; Kim, S. B.; Kim, S. I.; Park, S. M.; Jung, J. C.; Lee, K. H.; Ree, M. *Chem. Mater.* **2003**, *15*, 3105−3112.

(5) (a) Shin, T.; Park, H.; Lee, S.; Lee, B.; Oh, W.; Kim, J. S.; Baek, S.; Hwang, Y. T.; Kim, H. C.; Ree, M. *Polym. Eng. Sci.* **2003**, *43*, 1232−1240. (b) Chae, B.; Kim, S. B.; Lee, S. W.; Kim, S. I.; Choi, W.; Lee, B.; Ree, M.; Lee, K. H.; Jung, J. C. *Macromolecules* **2002**, *35*, 10119−10130. (c) Shin, T. J.; Ree, M. *Macromol. Chem. Phys.* **2002**, *203*, 791−800. (d) Shin, T. J.; Lee, B.; Youn, H. S.; Lee, K. B.; Ree, M. *Langmuir* **2001**, *17*, 7842−7850. (e) Lee, S. W.; Chang, T.; Ree, M. *Macromol. Rapid Commun.* **2001**, *22*, 941−947.

(6) Park, S.; Kim, K.; Kim, D. M.; Kwon, W.; Choi, J.; Ree, M. *ACS Appl. Mater. Interfaces* **2011**, *3*, 765−773.

(7) (a) Park, S.; Kim, K.; Kim, J. C.; Kwon, W.; Kim, D. M.; Ree, M. *Polymer* **2011**, *52*, 2170−2179. (b) Hahm, S. G.; Choi, S.; Hong, S. H.; Lee, T. J.; Park, S.; Kim, D. M.; Kwon, W. S.; Kim, K.; Kim, O.; Ree, M. *Adv. Funct. Mater.* **2008**, *18*, 3276−3282.

(8) Hahm, S. G.; Choi, S.; Hong, S. H.; Lee, T. J.; Park, S.; Kim, D. M.; Kim, J. C.; Kwon, W.; Kim, K.; Kim, M. J. *J. Mater. Chem.* **2009**, *19*, 2207−2214.

(9) Ling, Q. D.; Chang, F. C.; Song, Y.; Zhu, C. X.; Liaw, D. J.; Chan, D. S. H.; Kang, E. T.; Neoh, K. G. *J. Am. Chem. Soc.* **2006**, *128*, 8732−8733.

(10) Kim, K.; Park, S.; Hahm, S. G.; Lee, T. J.; Kim, D. M.; Kim, J. C.; Kwon, W.; Ko, Y. G.; Ree, M. *J. Phys. Chem. B* **2009**, *113*, 9143−9150.

(11) Kim, D. M.; Park, S.; Lee, T. J.; Hahm, S. G.; Kim, K.; Kim, J. C.; Kwon, W.; Ree, M. *Langmuir* **2009**, *25*, 11713−11719.

(12) Lee, T. J.; Chang, C. W.; Hahm, S. G.; Kim, K.; Park, S.; Kim, D. M.; Kim, J.; Kwon, W. S.; Liou, G. S.; Ree, M. *Nanotechnology* **2009**, *20*, 135204.

(13) (a) Chang, C. W.; Yen, H. J.; Huang, K. Y.; Yeh, J. M.; Liou, G. S. *J. Polym. Sci., Part A: Polym. Chem.* **2008**, *46*, 7937−7949. (b) Li, L.; Kikuchi, R.; Kakimoto, M. A.; Jikei, M.; Takahashi, A. *High Perform. Polym.* **2005**, *17*, 135−147. (c) Hsiao, S. H.; Liou, G. S.; Kung, Y. C.; Yen, H. J. *Macromolecules* **2008**, *41*, 2800−2808.

(14) (a) Bolze, J.; Ree, M.; Youn, H. S.; Chu, S. H.; Char, K. *Langmuir* **2001**, *17*, 6683−6691. (b) Bolze, J.; Kim, J.; Huang, J. Y.; Rah, S.; Youn, H. S.; Lee, B.; Shin, T. J.; Ree, M. *Macromol. Res.* **2002**, *10*, 2−12. (c) Hwang, Y.; Heo, K.; Chang, C. H.; Joo, M. K.; Ree, M. *Thin Solid Films* **2006**, *510*, 159−163.

(15) (a) Yoon, J.; Kim, K. W.; Kim, J.; Heo, K.; Jin, K. S.; Jin, S.; Shin, T. J.; Lee, B.; Rho, Y.; Ahn, B. *Macromol. Res.* **2008**, *16*, 575−585. (b) Lee, B.; Oh, W.; Hwang, Y.; Park, Y. H.; Yoon, J.; Jin, K.; Heo, K.; Kim, J.; Kim, K. W.; Ree, M. *Adv. Mater.* **2005**, *17*, 696−701. (c) Lee, B.; Park, Y. H.; Hwang, Y. T.; Oh, W.; Yoon, J.; Ree, M. *Nat. Mater.* **2005**, *4*, 147−150.

(16) (a) Yoon, J.; Jin, K. S.; Kim, H. C.; Kim, G.; Heo, K.; Jin, S.; Kim, J.; Kim, K. W.; Ree, M. *J. Appl. Crystallogr.* **2007**, *40*, 476−488. (b) Yoon, J.; Lee, S. W.; Choi, S.; Heo, K.; Jin, K. S.; Jin, S.; Kim, G.; Kim, J.; Kim, K. W.; Kim, H. *J. Phys. Chem. B* **2008**, *112*, 5338−5349. (c) Kim, G.; Park, S.; Jung, J.; Heo, K.; Yoon, J.; Kim, H.; Kim, I. J.; Kim, J. R.; Lee, J. I.; Ree, M. *Adv. Funct. Mater.* **2009**, *19*, 1631−1644.

(17) (a) Parratt, L. G. *Phys. Rev.* **1954**, *95*, 359−369. (b) Bolze, J.; Ree, M.; Youn, H. S.; Chu, S.-H.; Char, K. *Langmuir* **2001**, *17*, 6683−6691. (c) Hwang, Y.; Heo, K.; Chang, C. H.; Joo, M. K.; Ree, M. *Thin Solid Films* **2006**, *510*, 159−163.

(18) Campbell, A.; Bradley, D.; Lidzey, D. *J. Appl. Phys.* **1997**, *82*, 6326−6342.

(19) Jensen, K. L. *J. Vac. Sci. Technol., B* **2003**, *21*, 1528−1544.

(20) Mark, P.; Helfrich, W. *J. Appl. Phys.* **1962**, *33*, 205−215.

(21) (a) Frenkel, J. *Phys. Rev.* **1938**, *54*, 647. (b) Laurent, C.; Kay, E.; Souag, N. *J. Appl. Phys.* **1988**, *64*, 336−343.